International Journal of Heat and Mass Transfer 52 (2009) 4021–4030

Contents lists available at ScienceDirect

International Journal of Heat and Mass Transfer

journal homepage: www.elsevier.com/locate/ijhmt

Mathematical modeling of toxic pollutants dispersion from large tank fires and assessment of acute effects for fire fighters

N.C. Markatos *, C. Christolis, C. Argyropoulos

Computational Fluid Dynamics Unit, School of Chemical Engineering, National Technical University of Athens, 9, Iroon Polytechniou Str., Zografou Campus, GR - 157 80 Athens, Greece

ARTICLE INFO

Article history:
Received 5 December 2008
Aceepted by 23 March 2009
Available online 8 May 2009

Keywords:
Tank fire
Pollutant dispersion
Smoke plume
Turbulence
CFD
Risk zones

ABSTRACT

The paper presents a Computational Fluid Dynamics (CFD) approach to major – hazard studies, by applying a finite-domain technique to predict the dispersion of combustion products (CO, SO_2, smoke, Volatile Organic Compounds, VOC, Polycyclic Aromatic Hydrocarbons, PAH, etc.) from fuel-tank fires, as well as the toxic plume rise.

Furthermore, a methodology is presented for the identification of risk zones for the first respondents (fire fighters). Numerical simulations were performed with the use of the SIMPLEST algorithm, a second-order accurate MUSCL scheme with deferred correction for the convective terms in the momentum equations, CUPID for the convective terms in the scalar conservation equations, and a modified, RNG k-ε, two-equation turbulence model. Radiation was computed by a discrete transfer model. Various scenarios were examined and the results are presented and discussed.

1. Introduction

Many analysts, such as Beck [1], claim that we live in a society with many risks, which spread in all facets of our life. In the last 40 years, intense industrialization in the developed countries and the constant economic growth have brought new technologies, new products, new opportunities, better conditions of life, fast transportation and modern communications. However, there are also some indirect disadvantages from these improvements, including industrial accidents. Every year hundreds of work accidents, some with human losses and high cost for the economy and the environment, take place in the world.

Petrochemical industries normally use large storage tanks, which contain large amounts of flammable and hazardous chemicals. Hence, the occurrence of a tank accident is possible and it usually leads to fire and explosions. Experience has shown that the continuous dispersion of toxic pollutants from large tank fires, such as smoke, SO_2 and CO is responsible for potential environmental and health problems.

Industrial accidents such as that of February 24, 1986, in Thessaloniki, Greece, and the relatively recent large industrial accident of December 11, 2005 at Oil Storage Depots (Buncefield, Hertfordshire, England) demonstrated unanticipated consequences. The latter one produced a massive fire which engulfed over 20 large fuel-storage tanks. The continuous generation of smoke from these fires presents a potential environmental and health problem that is difficult to assess. In order to try and manage it, it is important to be able to estimate the concentration of the fire-plume pollutants over a wide range of conditions.

Hence, the need for new techniques and methodologies, in order to predict the consequences and to reduce the frequency of industrial accidents, is imperative. Refineries and chemical plants comprise the major part of storage-tank accidents, because of the large amounts of chemicals and fuels which are stored, mostly in atmospheric external floating-roof and cone-tap tanks.

According to the research of Chang and Lin [2], among the 242 tank accidents that have been reported in the last 40 years, the fire incident is the most frequent type of accident, caused by lightning and maintenance errors. Thus, the study of tank fires is of great importance, since, unfortunately, there is always a chance for a new accident. Under these circumstances, the fire plume produced from the burning fuel generates large amounts of toxic pollutants which are transported by the wind over a large area. The transportation of pollutants, such as sulfur dioxide (SO_2), carbon monoxide (CO), hydrogen sulfide (H_2S), as well as soot and particulates, have adverse effects on human health and the ecosystems.

Intensive research has been performed by many scientists and engineers for the investigation and explanation of the buoyant fire-plume dispersion. Ghoniem et al. [3] and Ghoniem and Zhang [4] have devised Lagrangian numerical techniques for the solution of governing equations, based on the extension of the vortex method to variable-density flows. Of a different numerical approach is the work of McGrattan et al. [5], with the use of Large Eddy Simulation (LES), for the simulation of turbulent smoke plume from large oil fires. Finally, Miles et al. [6], Christolis et al. [7], Sideris

* Corresponding author.
E-mail address: n.markatos@ntua.gr (N.C. Markatos).

0017-9310/$ - see front matter © 2009 Elsevier Ltd. All rights reserved.
doi:10.1016/j.ijheatmasstransfer.2009.03.039

Nomenclature

A_f	surface area of pool (m^2)
$C_{\varepsilon1}, C_{\varepsilon2}, C_{\varepsilon3}, C_\mu, \eta_o, \beta_1$	empirical constants in the turbulence model
g	gravitational acceleration (m/s^2)
G_B	buoyancy source/sink term
h	enthalpy (J/kg)
I	radiative intensity
IDLH	Immediate Dangerous to Life and Health
k	turbulence kinetic energy (m^2/s^2)
LC_1	Lethal Concentration
$\dot{m}''$	mass-loss rate (kg/s)
P	pressure (N/m^2)
P_k	turbulence kinetic-energy generation term
$\dot{q}$	volumetric heat-release rate ($J/(m^3s)$)
S	mean rate of strain
S_{ij}	deformation tensor
S_h	enthalpy source term (J/(kgs))
SP	source term of pollutants
T	temperature (K)
T_{ref}	reference temperature (K)
U_i	mean velocity component in the i-direction (m/s)
U_j	mean velocity component in the j-direction (m/s)
$\overline{U}$	average wind speed (m/s)
X, Y, Z	Cartesian co-ordinates
z_o	surface roughness (m)

Greek symbols

β	thermal expansion coefficient (1/K)
δ	height of atmospheric boundary layer
ε	turbulence dissipation rate (m^2/s^3)
n	ratio of turbulence time scale to mean strain-rate scale
φ	time-average of instantaneous flow variable
φ_P	value of flow variable at the central grid node, P
φ_I	value of flow variable at the neighbouring grid-node, I
ν	kinematic laminar viscosity ($kg/(m^2s)$)
ν_t	kinematic turbulence viscosity ($kg/(m^2s)$)
ρ	air density (kg/m^3)
σ_h	turbulence Prandtl number for enthalpy
σ_k	turbulence Prandtl number for kinetic energy of turbulence
σ_ε	turbulence Prandtl number for dissipation rate of turbulence
σ_T	turbulence Prandtl number for temperature
Ψ	Van Leer flux limiter

Subscripts

H	higher-order approximation
i, j	i, j directions
L	lower-order approximation
P	central grid node
ref	reference
t	turbulent
W	the node West of the central grid-node P
WW	the node west of the west-node of P

et al. [8] and Kefalas et al. [9] determined the "lift off" condition of buoyant fire plumes released from warehouses and buildings, using CFD techniques and the dimensionless buoyant-flux number.

The purpose of the present effort is to estimate the dispersion of combustion products and the consequences to the environment from large hydrocarbon-tank fires, as well as the height of the toxic plume (plume rise), and it is a continuation of the work by Argyropoulos et al. [10]. Furthermore, the risk zones for the first respondents, the fire fighters, are identified, by comparing the ground-level concentration of the pollutants with the safety limits. The mathematical model used in the present work consists of the full RANS (Reynolds-Averaged Navier–Stokes) differential equations that describe turbulent flow and heat and mass transport [11]. A MUSCL scheme [12] with deferred correction for the convective terms in the momentum equations, and the CUPID scheme [13] for the convective terms in the scalar conservation equations, were employed to discretize the equations and the solution was obtained using the iterative SIMPLEST algorithm of Spalding [14,15]. The RNG $k \sim \varepsilon$ model [16] was employed with the buoyancy modifications of Markatos and Pericleous [15], for the modeling of turbulence. Radiation is accounted for by a discrete transfer model [17,18].

Parametric analysis is performed for eight scenarios, all for an adiabatic atmosphere: for two different fuels with heat-release rates of 1 and 1.3 MW/m^2, and for four values of wind velocity, 7, 8, 9 and 11 m/s.

2. The physical problem considered

For the numerical simulation of the toxic contaminants dispersion and of the plume rise, an external floating-roof tank has been selected, with dimensions of 85 m diameter and of 20 m height. The tank is surrounded by bunds of 4 m height and 0.5 m width. The geometry of the tank with the bund is illustrated in Fig. 1.

This type of tank is characterized by the ability of the roof to rise and fall on the stored-fuel surface, according to the latter level, with a maximum storage capacity of 113,432 m^3. Numerical simulations were performed with the use of CFD techniques for a physical domain of 30000 m length (Z-axis), 2200 m width (X-axis) and 2500 m height (Y-axis). These dimensions were chosen following a parametric study, in order to evaluate the extent of the domain

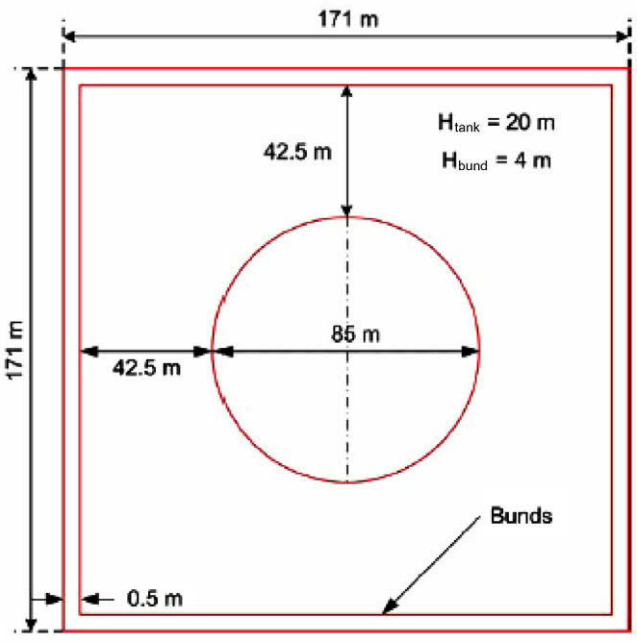

Fig. 1. The tank geometry considered.

after which no major change of the variables was computed close to the tank. *Z*-axis is the parallel to the wind direction axis, *X*-axis is the vertical to the wind direction on the ground-level axis, while *Y*-axis is the vertical axis. The tank is situated 543 m from the origin of the *Z*-axis and 1100 m from the *X*-axis (symmetry).

3. The mathematical model

3.1. Governing equations

The mathematical model is based on the set of elliptic, partial-differential equations (PDE) expressing the conservation of mass, momentum, chemical species, enthalpy and two turbulence variables in steady, three dimensional flow. Assumptions adopted for the flow equations are that the Coriolis force is negligible and that the Boussinesq approximation is valid. The steady-state, 3D equations with buoyancy forces can be written in Cartesian-tensor notation as follows:

Continuity equation:

$$\frac{\partial U_i}{\partial x_i} = 0 \tag{1}$$

Momentum equations:

$$U_j \frac{\partial U_i}{\partial x_j} = -\frac{1}{\rho}\frac{\partial p}{\partial x_i} + \frac{\partial}{\partial x_j}\left[(\nu + \nu_t)\left(\frac{\partial U_i}{\partial x_j} + \frac{\partial U_j}{\partial x_i}\right)\right] + g_i\left(\frac{T - T_{ref}}{T_{ref}}\right) \tag{2}$$

Energy equation:

$$U_j \frac{\partial h}{\partial x_j} = \frac{\partial}{\partial x_j}\left\{\left(\frac{\nu}{P_r} + \frac{\nu_t}{\sigma_h}\right)\frac{\partial h}{\partial x_j}\right\} \tag{3}$$

Chemical species concentration equation:

$$U_j \frac{\partial C}{\partial x_j} = \frac{\partial}{\partial x_j}\left\{\left(\nu + \frac{\nu_t}{\sigma_C}\right)\frac{\partial C}{\partial x_j}\right\} \tag{4}$$

where ρ is the fluid density, U_j the velocity vector, p the pressure, g_i the gravitation acceleration, T_{ref} the reference temperature, equal to 298 K, T the temperature, ν the kinematic viscosity, ν_t is the Boussinesq eddy viscosity, h is the enthalpy, P_r the Prandtl number, σ_h the "turbulence" Prandtl number for h, C the concentration of chemical species and σ_C is the "turbulence" Schmidt number for C. The subscripts i, j(=1–3) denote the three space coordinates.

Since for the cases under consideration buoyancy plays an important role in promoting turbulent mixing, the RNG $k \sim \varepsilon$ model (Yakhot and Orszag, [16]) was employed with the modifications of Markatos and Pericleous [15], in order to account for buoyancy forces in the production/destruction of the kinetic energy of turbulence. The selection of RNG $k \sim \varepsilon$ model was preferred to the standard one as, according to the work of Kim and Patel [19] but also according to our experience, it was shown to give the best prediction of pollutant dispersion under neutrally stratified atmosphere. Hence, the turbulence kinetic energy k and its dissipation rate ε, obey the following transport equations:

Equation for kinetic energy of turbulence (k):

$$U_j \frac{\partial k}{\partial x_j} = \frac{\partial}{\partial x_j}\left\{\left(\nu + \frac{\nu_t}{\sigma_k}\right)\frac{\partial k}{\partial x_j}\right\} + P_k + G_b - \varepsilon \tag{5}$$

Equation for dissipation rate of turbulence (ε):

$$U_j \frac{\partial \varepsilon}{\partial x_j} = \frac{\partial}{\partial x_j}\left\{\left(\nu + \frac{\nu_t}{\sigma_\varepsilon}\right)\frac{\partial \varepsilon}{\partial x_j}\right\} + (c_{\varepsilon 1}P_k - c_{\varepsilon 2}\varepsilon + c_{\varepsilon 3}G_b)\frac{\varepsilon}{k} - \frac{c_\mu \eta^3(1 - \eta/\eta_0)}{1 + \beta_1 \eta^3}\frac{\varepsilon^2}{k} \tag{6}$$

where σ_k and σ_ε are Prandtl numbers for k and ε, respectively, and $C_{\varepsilon 1}$, $C_{\varepsilon 2}$, $C_{\varepsilon 3}$, C_μ, n_0 and β_1 are the model "constants". Herein, P_k signifies the production rate of turbulence kinetic energy, G_b is the term of production of turbulence energy due to the action of buoyancy forces, η is the ratio of the turbulence time scale to the mean strain-rate scale, and ν_t is the Boussinesq eddy viscosity. P_k, G_b, η and ν_t are given by the following equations, and the values of the model constants are presented in Table 1.

Table 1
Values of RNG $k \sim \varepsilon$ model constants [16].

$C_{\varepsilon 1}$	$C_{\varepsilon 2}$	$C_{\varepsilon 3}$	C_μ	σ_k	σ_ε	n_o	β_1
1.42	1.68	tanh/uv	0.0845	0.719	0.719	4.38	0.012

$$P_k = \nu_t\left(\frac{\partial U_i}{\partial x_j} + \frac{\partial U_j}{\partial x_i}\right)\frac{\partial U_i}{\partial x_j} \tag{7}$$

$$G_b = -g\frac{1}{T_{ref}}\frac{\nu_t}{\sigma_T}\frac{\partial T}{\partial y} \tag{8}$$

$$\nu_t = c_\mu \frac{k^2}{\varepsilon} \tag{9}$$

$$\eta = \frac{Sk}{\varepsilon} \tag{10}$$

where in Eq. (10) S denotes the mean strain-rate of the flow, defined as:

$$S^2 = (2S_{ij}S_{ij}) \tag{11}$$

where the deformation tensor, S_{ij} is expressed as:

$$S_{ij} = \frac{1}{2}\left(\frac{\partial U_i}{\partial x_j} + \frac{\partial U_j}{\partial x_i}\right) \tag{12}$$

3.2. Boundary conditions

Boundary conditions are specified as follows. A logarithmic profile was used at the inlet boundary for the wind velocity within the atmospheric boundary layer, and then it was kept constant above that height. The logarithmic profile is defined by the following equation (Tennekes [20]):

$$\overline{U} = \frac{u_*}{k_a}\ln\left(\frac{z}{z_0}\right) \tag{13}$$

Here $\overline{U}$ is the average wind speed at height z, k_a is the von Karman constant (=0.41), u^* is the friction velocity and z_0 the roughness height of the surface. Friction velocity u^* is estimated by inserting a known reference wind speed into Eq. (13). The reference wind speed at 10 m above the surface is applied, being a standard height for wind measurements. The surface roughness, z_0, is taken as 0.3 m for urban environment; and at the top of the boundary the normal change of all variables is set to zero. Finally, outside the flow field the external pressure is considered uniform.

At the inlet boundary the profile of turbulence kinetic energy (k) is calculated by the equation of Huser et al. [21] and the dissipation rate of turbulence (ε) is estimated by Eqs. (16) and (17), below

Turbulence kinetic energy (k):

$$k = \frac{u_*}{\sqrt{C_\mu}}\left(1 - \frac{z}{\delta}\right) \quad \text{for} \quad z \le 0.9\delta \tag{14}$$

$$k = 0.1\frac{u_*}{\sqrt{C_\mu}} \quad \text{for} \quad z > 0.9\delta \tag{15}$$

Dissipation rate of turbulence (ε):

$$\varepsilon = \frac{C_\mu^{3/4}k^{1.5}}{k_a z} \quad \text{for} \quad z \le 0.22\delta \tag{16}$$

$$\varepsilon = \frac{C_\mu^{3/4}k^{1.5}}{k_a \delta} \quad \text{for} \quad z > 0.22\delta \tag{17}$$

where δ is the height of the atmospheric boundary layer. In this work the atmospheric stability has been selected to be of class *D*, which represents neutral conditions. Another important parameter for the dispersion of pollutants is the height of the atmospheric boundary layer, δ, the value of which has been taken as equal to 800 m.

At solid boundaries of the physical domain, the no-slip condition is imposed and zero-flux conditions were applied at the symmetry plane for all variables. Moreover the momentum flux to the walls is considered to obey the "wall-function" relationships of Launder and Spalding [22].

3.3. The radiation model

The basis of all methods for the solution of radiation problems is the radiative transfer equation (RTE) [17,18]:

$$\underline{s}\cdot\nabla I(\underline{r},\underline{s}) = -\kappa(\underline{r})I(\underline{r},\underline{s}) + Q(\underline{r},\underline{s}) \tag{18}$$

which describes the radiative intensity field, *I*, within the domain, as a function of location vector ($\underline{r}$) and direction vector ($\underline{s}$); Q represents the total attenuation of the radiative intensity due to the gas emission and to the in-scattered energy from other directions to the direction of propagation, and κ is the total extinction coefficient.

The discrete transfer model of Lockwood and Shah [18] discretizes the RTE along rays. The path along a ray is discretized by using the sections formed from breaking the path at zone boundaries. Assuming that the physical properties remain constant inside a zone, Eq. (18) can be integrated from zone entry to zone exit (Fig. 2) to yield:

$$I_{n+1} = I_n e^{-\tau_n} + L_n Q_n\left[\frac{1-e^{\tau_n}}{\tau_n}\right]; \quad \tau_n = \kappa L_n \tag{19}$$

where L_n is the path length in the *n*-th zone, I_n and I_{n+1} are the intensities at zone entry and zone exit, respectively, and:

$$Q_n(\underline{r},\underline{s}) = \frac{k_a}{\pi}\sigma T_n^4 + k_s J_n(\underline{r}) \tag{20}$$

where k_a, k_s, are the absorption and scattering coefficients for a gray medium, $J_n(\underline{r}) = \frac{1}{4\pi}\int I_n(\underline{r},\underline{s})d\Omega$ is the mean intensity of the in-scattered radiation, σ is the Stefan-Boltzmann constant and $d\Omega$ is the element of solid angle containing *s*.

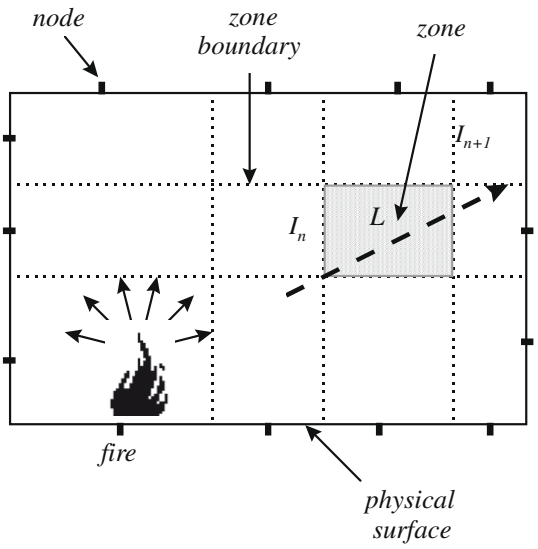

Fig. 2. Sub-division of the solution domain into zones.

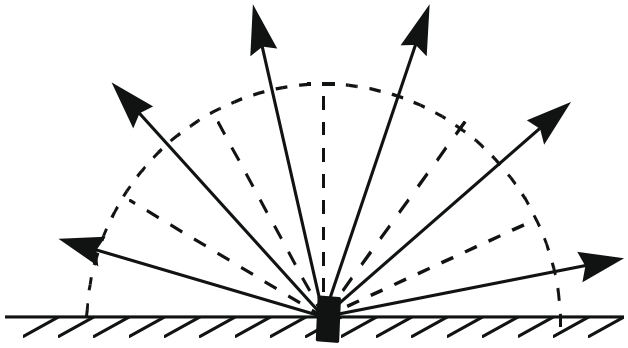

Fig. 3. Projection of a ray at a node into a number of angular divisions.

The rays are chosen by fixing nodes to all the physical surfaces, dividing up the interior hemisphere into elements of equal solid angle and projecting one ray into each solid angle (Fig. 3).

For gray surfaces, integration of Eq. (18) yields the required boundary conditions:

$$I(\underline{r},\underline{s}) = \frac{e_W}{\pi}\sigma T^4(\underline{r}) + \frac{1-e_W}{\pi}R(\underline{r}) \tag{21}$$

where e_W is the wall emissivity, and $R(\underline{r}) = \int_{\underline{s}\cdot\underline{n}<0}(\underline{s}\cdot\underline{n})I(\underline{r},\underline{s})d\Omega$ is the radiation flux on a surface, and *n* is the inward pointing unit vector normal to the surface at *r*.

The spectral nature of radiation is generally considered to be important in combustion processes. The error introduced by the assumption of a gray gas cannot be a priori estimated; however, evaluation, of the final results (see Section 5.4 below) indicates that in the present case it may be only a few percent.

3.4. Heat and mass sources of fire and toxic contaminants

3.4.1. Estimation of heat-release rate and mass burning rate of the fuels

The computational work required for the present application is very demanding in terms of CPU time. Therefore, the use of detailed chemistry modeling was avoided. Instead, the heat and mass source of the fire on the surface of the external floating-roof tank is simulated as a volumetric source, which releases heat at a constant rate. Hence, the fire on the top of the external floating-roof tank is characterized as a large pool fire. Thus, the estimation of mass loss rate $\dot{m}''$ and the total heat-release rate $\dot{q}$ (HRR) are important input parameters for the model. The calculation of the above quantities is determined by the following expressions (Babrauskas [23]):

$$\dot{m}'' = \dot{m}''_\infty(1-e^{-\kappa\beta D}) \tag{22}$$

$$\dot{q} = \dot{m}''\Delta H_{c,eff}A_f \tag{23}$$

where $\dot{m}''_\infty$ is the infinite-diameter pool mass-loss rate, k is the absorption extinction coefficient of the flame, β is a "mean beam length corrector", D is the pool diameter, $\Delta H_{c,eff}$ is the heat of combustion and A_f is the surface area of the pool. In this study the type, HRR and mass burning rate of fuels and the appropriate values for the $\dot{m}''_\infty$, k, β and $\Delta H_{c,eff}$ have been adopted from the work of Babrauskas [23]. The mass burning rate for both liquid fuels used has been calculated for steady-state conditions, even though the mass burning rates vary with time.

The estimated value of HRR for all accident scenarios presented here (Table 2) has been calculated from the total HRR, which is estimated from Eq. (23), minus the computed thermal radiation.

3.4.2. Emission factors for the toxic contaminants of the fuels

Combustion products of various fuels are characterized by the presence of toxic pollutants such as smoke, sulfur dioxide (SO_2),

Table 2
Accident scenarios with plume rise estimation.

Scenarios	Fuel	HRR (MW/m^2)	Wind velocity (m/s)	Plume rise (m)
(1)	Crude oil	1	8	1746
(2)	Crude oil	1	11	1335
(3)	Diesel	1.3	8	1781
(4)	Diesel	1.3	11	1417

carbon dioxide (CO_2), carbon monoxide (CO), etc. The prediction of their ground-level concentration is of great importance for this study, in order to assess its impact on human health.

In the present study, two fuels have been examined, crude oil and diesel oil, and the ground-level concentration of smoke, CO, SO_2, Polycyclic Aromatic Hydrocarbons (PAH) and Volatile Organic Compounds (VOC) have been estimated.

Unfortunately, experimental data for large-scale pool fires with diameter 85 m are not available. Many attempts from various researchers (Notarianni et al. [24]; Koseki et al. [25]; Evans et al. [26]; Walton et al. [27]) have been performed in the hope of studying the phenomenon but without prospective results, because of the complexities of the physical problem. The fire experiments have been conducted for various pool fire sizes of 5, 10, 15, 17, 20 and 50 m diameter.

Because of the absence of experimental data for the emission factors of pollutants, available data from the literature have been used. More specifically, laboratory data have been adopted in meso-scale and offshore burning experiments (Notarianni et al. [24]; Koseki et al. [25]; Evans et al. [26]; Walton et al. [27]; Booher and Janke, [28]; Lemieux et al. [29]). Then, with the appropriate data for emission factors, it has been easy to calculate the source term of the pollutants for the model. Thus, the source term of the pollutants is estimated by the following equation:

$$SP = \dot{m}'' \times EF \times A_f \tag{24}$$

where SP is the source term of the pollutant, $\dot{m}''$ is the mass burning rate of the fuel, EF is the emission factor of the pollutant for the specific fuel and A_f is the area of pool fire.

3.4.2.1. Crude oil. Crude oil contains both hydrocarbons and different compounds containing nitrogen, oxygen, hydrogen, sulfur and metals. The liquid quantity used in the numerical simulation was set equal to the capacity of the tank, and the density was 880 kg/m^3 (Babrauskas [23]).

According to the evidence of the works of Evans et al. [26] and Walton et al. [27] the value of smoke yield for crude oil appears to be from 10% to 15%. Herein, the value of smoke yield is taken equal to 12.5% which is the average of the above measurements. The source term for smoke is calculated with the help of Eq. (24) and is equal to 24.1 kg/s.

The emission factor for CO is taken equal to 0.09 kg CO/kg fuel according to the evidence of Evans et al. [26] and Evans [30]. For SO_2, the value of emission factor depends on the sulfur content of the fuel and it is taken equal to 0.04 kg SO_2/kg fuel. PAHs and VOCs emissions factors are adopted from the research of Booher and Janke [28] and their values are 0.0004 kg PAHs/kg fuel and 0.0005 kg VOCs/kg fuel, respectively.

3.4.2.2. Diesel oil. Diesel oil is composed of about 75% saturated hydrocarbons and 25% aromatic hydrocarbons. Similar to the assumptions for the crude oil, the smoke yield for diesel oil varies from 15% up to 20% (Walton et al.). Herein, the value of smoke yield is taken equal to 17.5%, which is the average of the above values from the literature.

In the present work the emission factor for estimating the concentration of sulfur dioxide (SO_2) for diesel is based on the sulfur content of the fuel, as for the crude oil, and the value is 0.02 kg SO_2/kg fuel. Finally the emission factors for CO, PAHs and VOCs are adopted from the research of Booher and Janke [28] and their values are taken equal to 0.03 kg CO/kg fuel, 0.0009 kg PAHs/kg fuel and 0.0004 kg VOCs/kg fuel, respectively.

4. Method of solution

4.1. Solution procedure and grid sensitivity analysis

The set of the model partial-differential equations, along with the appropriate boundary conditions and the auxiliary relations have been solved by means of the Finite Volume Method (Patankar and Spalding [31]).

The model is implemented in the general computer program PHOENICS (Spalding [32]).

The treatment of the convective terms in conservation equations determines the accuracy of the solutions. These terms are difficult to handle numerically because the more accurate schemes tend to be less robust and/or slower to converge. Consider the control volume shown in Fig. 4. The scheme used here is illustrated taking an example of the west face (w), for variable φ.

Monotone Upstream-Centered Schemes for Conservation Laws (MUSCL) [12] are modifications to the higher-order upwind scheme with flux limiters to ensure boundedness and monotonicity of the solution. In this work a second-order MUSCL scheme is used as follows:

$$\Phi_w = \left(1 + \frac{1}{2}\Psi\right)\Phi_W - \frac{1}{2}\Psi\Phi_{WW} \tag{25}$$

Where Ψ is the flux limiter which is given in terms of the ratio:

$$r = \frac{\Phi_P - \Phi_W}{\Phi_W - \Phi_{WW}} \tag{26}$$

Van Leer's flux limiter is used [33]:

$$\Psi = (r + |r|)/(1 + |r|) \tag{27}$$

and deferred correction was applied:

$$\Phi_w = \Phi_w^L + a(\Phi_w^H - \Phi_w^L)^{old} \tag{28}$$

where Φ_w^L stands for the usual first-order upwind approximation and Φ_w^H for the above Van Leer approximation. The term in brackets is evaluated using values from the previous iteration, as indicated by the superscript "old". Although this term is obviously small com-

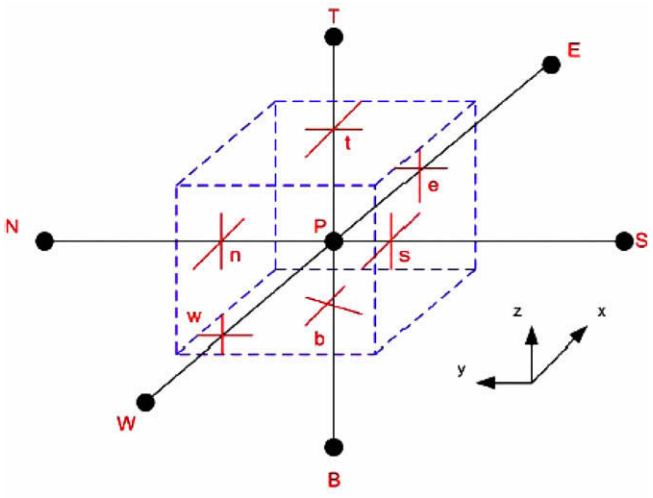

Fig. 4. The control volume.

pared to Φ_w^L, the factor α that blends the two schemes is taken here as 0.4, in order to diminish further the explicit treatment, thus improving convergence.

An attempt was also made to use CUPID [13], that intuitively appears well suited, but convergence was not obtained when it was used for the momentum equations; its use was thus restricted to the equations of the scalar variables.

In addition, the computational domain was divided into regions for the better simulation of the phenomenon in each space dimension. The selection of the appropriate grid for the numerical simulation was based on a grid sensitivity analysis among various different grids, between 2 and 5 million cells. It was found that the results of grids $66 \times 156 \times 248$, $70 \times 167 \times 260$ and $80 \times 190 \times 280$ were sufficiently close to each other. Therefore, the grid of $66 \times 156 \times 248$(2,553,408 cells) was used for the final runs, as the results were virtually grid-independent and the computational cost significantly lower than for the finer grids.

4.2. Convergence and time requirements

Runs were performed on a Linux PC with CPU 2.8 GHz and main memory of 1 Gbytes. Convergence was achieved by applying under-relaxation techniques. More specifically, the following criterion for all dependent variables was met:

$$\max|\phi^{n+1} - \phi^n| \leq 10^{-4} \tag{29}$$

between sweeps n and n+1. The "false transient" type of relaxation was used for the velocity components, enthalpy and concentration of chemical species, the value of "false time step" taken equal to 0.1. For pressure and turbulence the usual "linear" type of relaxation was employed with a value of 0.30. About 10,000 sweeps of the computational domain were needed to ensure full convergence for the grid of $66 \times 156 \times 248$ (2,553,408 cells). The CPU time required was about 200 h.

5. Results and discussion

The overwhelming amount of results obtained dictates a judicious choice of some of them for presentation. The results are presented below, according to the author's judgement of what is practically meaningful, and are discussed under headings of plume rise, ground-level concentrations and hazard identification.

Figs. 5–7 present velocity vectors and enthalpy contours around the tank on fire. These figures show clearly the way the flow develops (magnitude and direction) and the location of the highest temperatures.

5.1. Plume rise analysis

Plume rise analysis was performed for four different scenarios. More specifically, crude oil and diesel are examined with two values of wind velocity, 8 and 11 m/s. Table 2 presents the general characteristics of four accident scenarios with the results from the calculation of plume rise for all cases and Fig. 8 illustrates the center line curve of the plume downwind from the center of the tank for each scenario. The plume axis is specified by tracing the location of the maximum concentration at each vertical z-slab.

According to the results from the four accident scenarios the highest plume rise occurs for scenario (3), at 1781 m. This is due to the highest HRR (1.3 MW/m^2) strength of the fire and lowest wind velocity (8 m/s), compared with the other scenarios. Therefore, the buoyancy forces are strong enough and with the help of medium-speed wind the plume is transported high in the atmospheric boundary layer.

On the other hand, the lowest plume trajectory takes place in scenario (2), at the height of 1335 m. This attitude is explained by the lowest HRR (1 MW/m^2) strength of fire and the highest value of wind velocity (11 m/s) among the other scenarios. Thus, the buoyancy forces are not strong enough to raise the plume and, due to the high wind velocity (11 m/s), the plume is transported to the ground-level with anticipated consequences for the environment and human health.

5.2. Ground-level concentration

The estimation of the anticipated consequences from the toxic contaminants is usually based on the ground-level concentration of these toxic gases after dispersing. For all accident scenarios, ground-level concentration is examined for two zones at a height of 1 m from the ground. The first zone lies closer to the tank fire and has a range of approximately 1000–1500 m from the tank and the pollutant concentrations there are rather high. The second zone is further away from the tank and follows the first zone up to the end of the domain. The toxic contaminants concentrations are

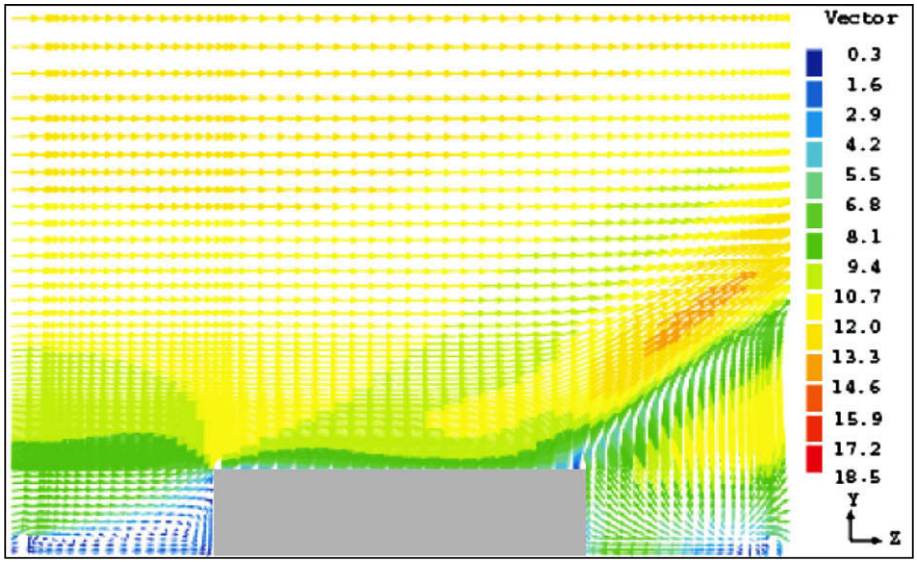

Fig. 5. Velocity vectors (*YZ* plane).

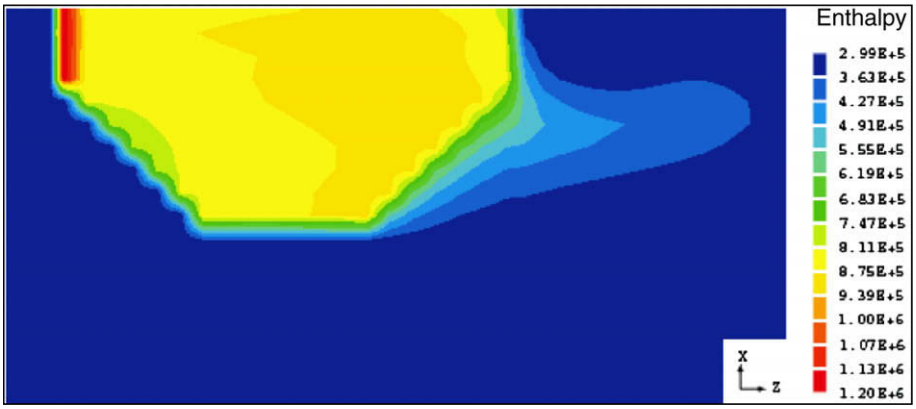

Fig. 6. Enthalpy contours (XZ plane).

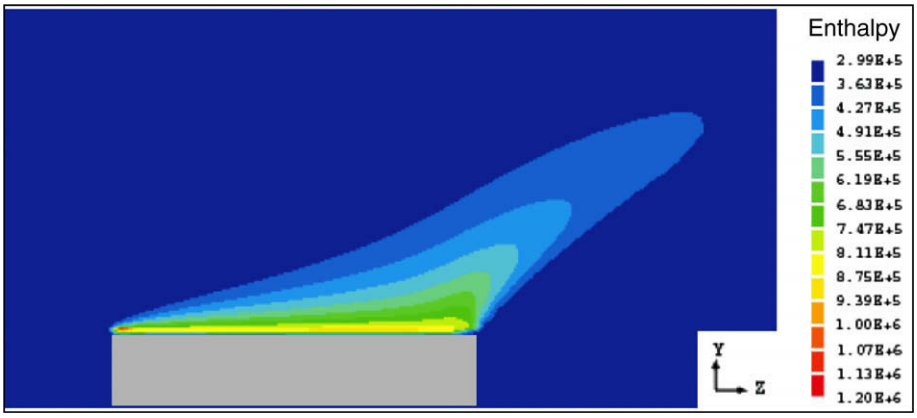

Fig. 7. Enthalpy contours (*YZ* plane).

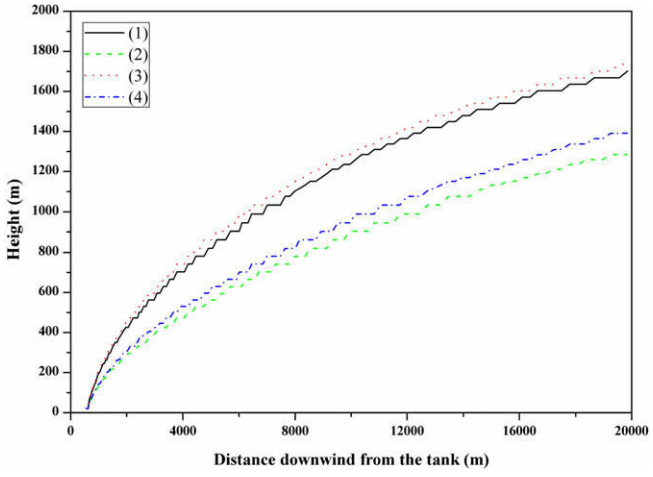

Fig. 8. Plume rise vs. the downwind distance from the tank for each scenario.

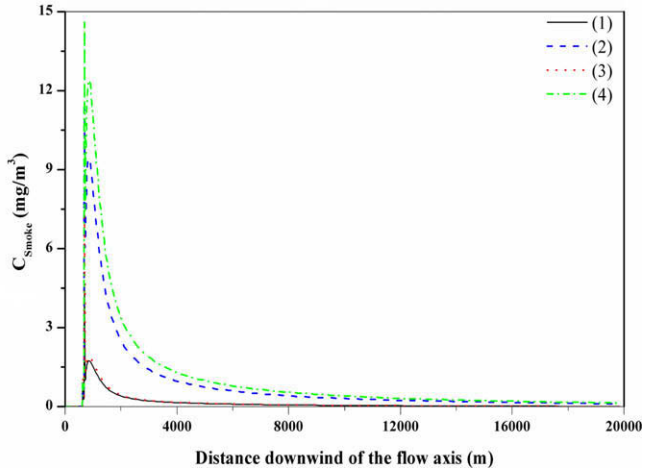

Fig. 9. Ground-level concentrations of smoke for all scenarios at 1 m height from the ground.

lower, but it is still possible to be significant depending on the toxic characteristics of the fuel.

From the parametric analysis it is concluded that the worst-case scenario, among the four scenarios which were examined, for smoke ground-level concentration is scenario (4) and the lowest smoke concentration appears for scenario (1).

The above results are shown in Fig. 9 and it is seen that the ground-level concentrations of smoke in the first zone near to the tank are in the range of 3–15 mg/m^3, which are very high. The values in the second zone are small and range from 0 to 3 mg/m^3. Substantial differences in ground-level concentrations of smoke depend also on the fuel because of the different % smoke yield.

According to Fig. 10, it is observed that CO emissions for scenario (2) are the highest, while the lowest values appear for scenario (3). In the first zone, near to the tank, the ground-level concentrations of CO present high values within a range of

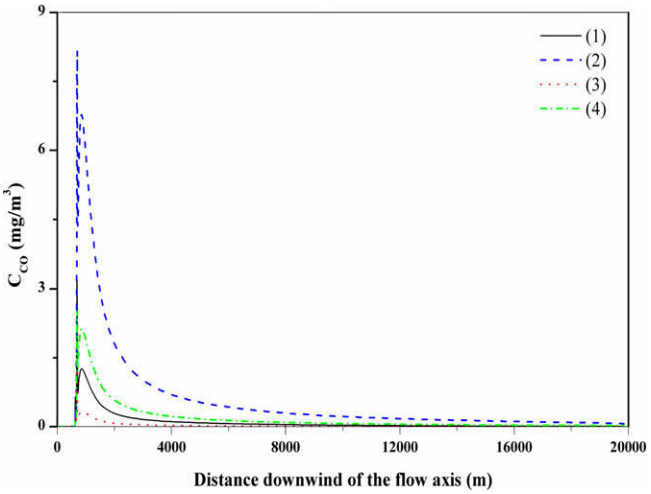

Fig. 10. Ground-level concentrations of CO for all scenarios at 1 m height from the ground.

2–8 mg/m^3, while the range of values for the second zone, away from the tank, is from 0 to 2 mg/m^3. An important factor of these differences between the ground-level concentration of crude oil and diesel is the emission factor of CO which is different for the two fuels.

Moreover, in Fig. 11 for SO_2 emissions, scenario (2) presents the highest ground-level concentration and scenario (3) the lowest. Similar to the above situations, the ground-level concentrations for SO_2 in the first zone are extremely high, with concentration values from 1.5 to 3.8 mg/m^3. In the second zone the values for SO_2 emissions are very low, from 0 to 1.5 mg/m^3.

From the above Figs. 9–11, it is observed that for all ground-level concentrations of pollutants, except for smoke, scenario (2) gives the highest values of concentration and scenario (3) the lowest.

Moreover, Figs. 12–14 illustrate concentration of smoke, CO and SO_2 profiles taken at 5 km perpendicular to the flow axis.

It is observed that for low heights the concentrations of smoke, CO and SO_2 are extremely high at a position 5 km downwind of the flow axis. On the contrary, with the increase of height the concentrations of smoke, CO and SO_2 decrease.

In Fig. 12, it is noticed that for heights in the range of 500–750 m above the ground-level, the value of maximum concentration of smoke is 9 mg/m^3. Scenario (4) presents the maximum value of smoke concentration. The lowest value of smoke concentration is observed for scenario (1) and it is equal to 4 mg/m^3 at a height of 800 m.

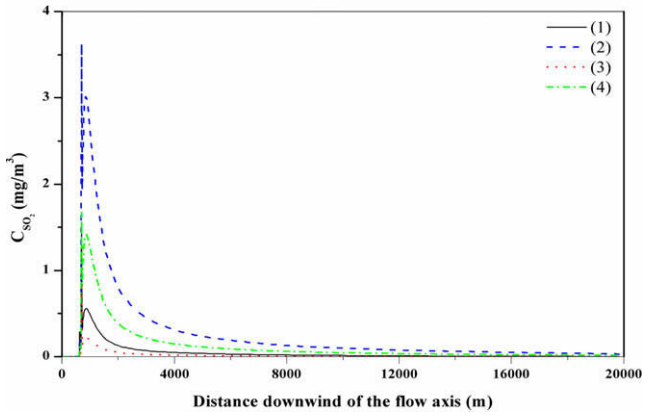

Fig. 11. Ground-level concentrations of SO_2 for all scenarios at 1 m height from the ground.

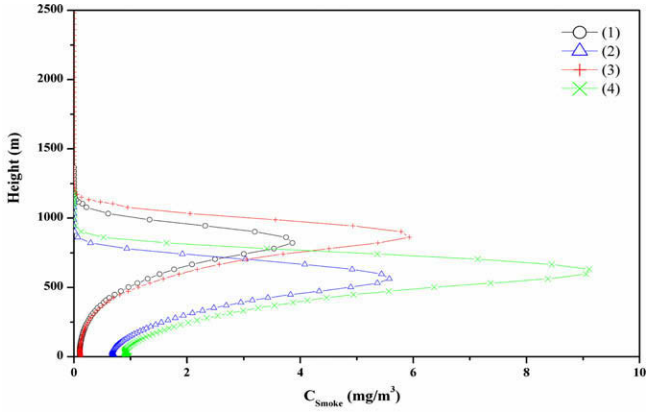

Fig. 12. Concentration of smoke vs. the height at a position of 5 km from the flow axis.

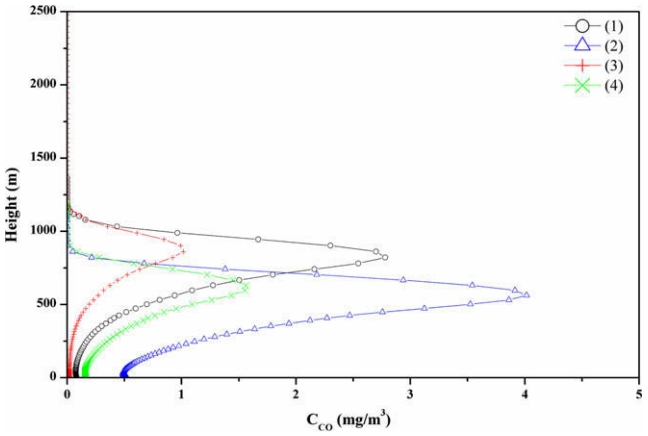

Fig. 13. Concentration of CO vs. the height at a position of 5 km from the flow axis.

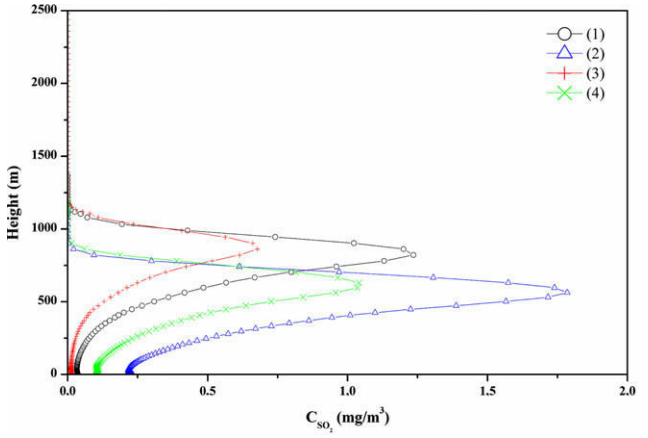

Fig. 14. Concentration of SO_2 vs. the height at a position of 5 km from the flow axis.

In Fig. 13, it is observed that the maximum value for CO concentration is found for scenario (2) and is equal to 4 mg/m^3. On the other hand the minimum value appears for scenario (3) and it is 1 mg/m^3, approximately.

Finally, in Fig. 14, the same behaviour is exhibited for the concentration of SO_2, the maximum value found for scenario (2) and

the minimum value for scenario (3), with values of 1.8 and 0.7 mg/m^3, respectively.

5.3. Hazard identification analysis

Hazard identification analysis is performed with the characterization of risk zones (Fig. 15), by comparing the ground-level concentration of the pollutants with the safety limits.

The present methodology for the determination of hazard range can be described by comparing the ground-level concentrations of the pollutants (smoke, CO, SO_2) with the Lethal Concentration (LC_1) and Immediately Dangerous to Life and Health (IDLH) values of them [9]. The (LC_1) determines the range of the high-risk zone where only fire fighters are allowed wearing the appropriate gear, and (IDLH) specifies the hazard range for the general population [9]. The values for the above safety limits are adopted from the National Institute for Occupational Safety and Health (NIOSH) web site (http://www.cdc.gov/niosh/homepage.html). The LC_1 (CO) = 9190.18 mg/m^3 and IDLH (CO) = 1374.23 mg/m^3, for SO_2 LC_1 (SO_2) = 2525.97 mg/m^3 and IDLH (SO_2) = 262 mg/m^3. Limit values for smoke are LC_1 (smoke) = 25,000 mg/m^3 and IDLH (smoke) = 2500 mg/m^3.

From the parametric runs above, the ground-level concentrations of toxic pollutants for the two zones are computed for all scenarios. According to those data, there are no "death zones" due to the concentrations of smoke, CO and SO_2. In the first zone the concentrations which are observed are high, especially for smoke, but do not exceed the safety limits of LC_1 or IDLH.

5.4. Some further results

It is interesting to point out that comparison with earlier work by the author and his colleagues [10], reveals that despite the present more sophisticated treatment of the convective terms (use of Van Leer and CUPID Schemes rather than the hybrid one of Spalding [34]), and the detailed calculation of the radiation effects, the results do not differ by more than 7–8%, with maximum of 10% for the enthalpy. In [10] the estimated value of HRR for all scenarios was calculated from the total HRR (Eq. (23)), minus the fraction of thermal radiation, which constitutes a 30% of the total HRR, according to literature [35]. A rough calculation of present computed radiation contribution reduces this fraction to 20%, which may be attributed to the very large fire diameter that leads to smoke obscuration [35].

In total 18 scenarios were run for different fire strengths and wind speeds. Some results concerning the effect of the tank diam-

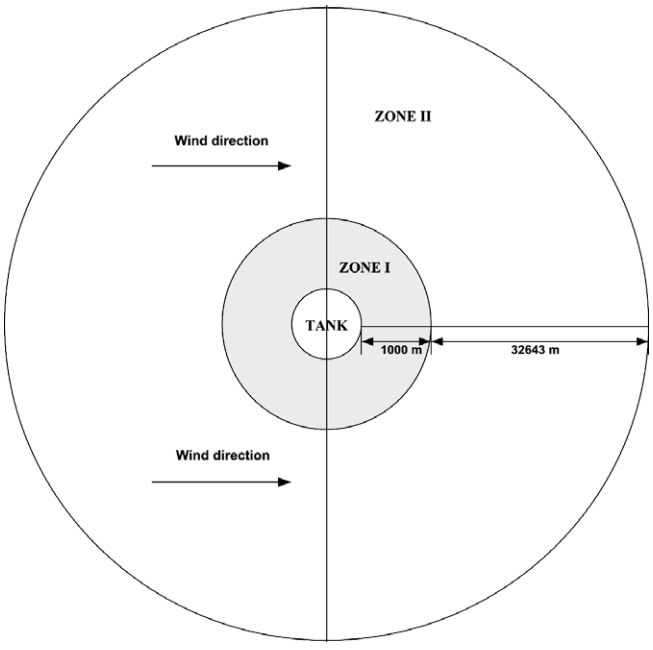

Fig. 15. Configuration of risk zones.

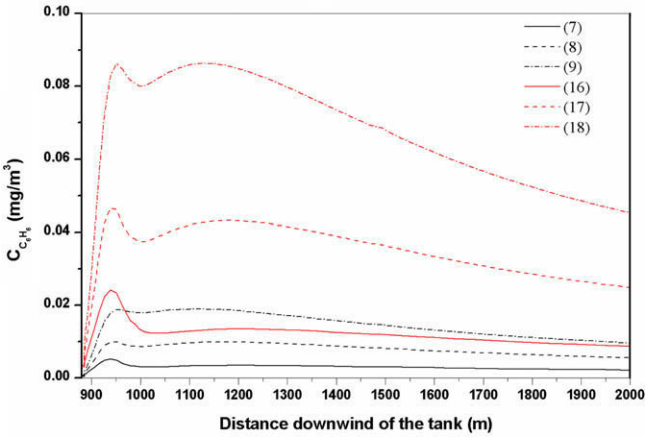

Fig. 16. Ground-level concentration of benzene at 1 m height from the ground for various scenarios. Tank diameter is 50 m.

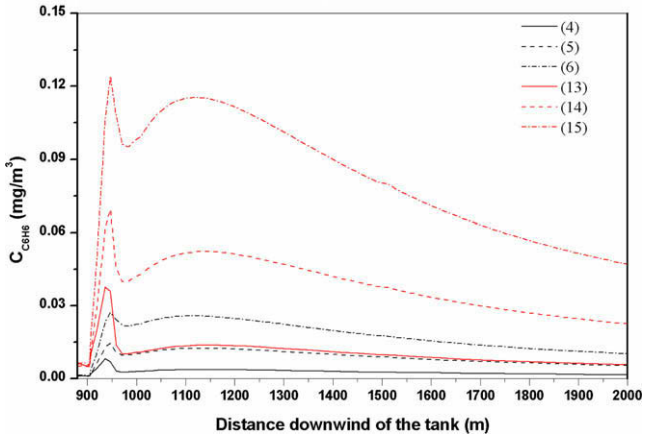

Fig. 17. Ground-level concentration of benzene at 1 m height from the ground for various scenarios. Tank diameter is 70 m.

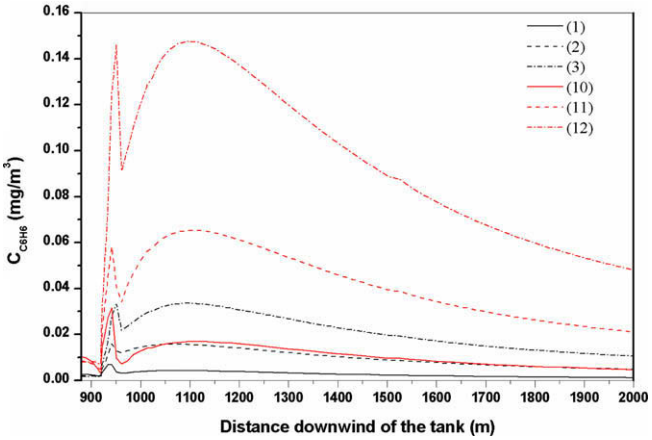

Fig. 18. Ground-level concentration of benzene at 1 m height from the ground for various scenarios Tank diameter is 85 m.

eter on the pollutants ground concentration are shown in Figs. 16–18. It is seen that the larger the diameter the higher the pollutant concentration and the more abrupt the slope of its distribution with distance downwind.

6. Conclusions

The work described herein focuses on the computation of toxic contaminant releases from large hydrocarbon-tank fires. An integrated methodology is developed and applied in order to quantify the consequences. The cases studied were four accident scenarios with different HRR and wind velocities. The available data were inadequate for the detailed description of the accident scenarios and several assumptions had to be made, concerning the input data, based on the worst-case scenario.

Fires of great diameter in storage tanks of liquid fuels, such as crude oil, kerosene, etc., are very difficult to be extinguished. This means that the fire may burn for days until all the fuel in the tank is burnt. In these cases the dispersion of the plume and toxic pollutants depends on the meteorological conditions and the characteristics of the fire. The most serious consequences are exhibited for high wind velocity and weak fire, i.e., when the plume is trapped very close to the ground with high values of pollutant concentrations. On the contrary, with low wind velocity and strong fire, the plume of smoke is dispersed at great heights away from the ground and the pollutant concentrations decrease. It is also concluded that, for the accident scenarios considered, there are no "death zones" due to the concentrations of smoke, CO and SO_2 and that near and away from the tank, the safety limits are not exceeded.

The results have been shown to be physically reasonable. The author believes that the results shown in this paper, and the far greater number of similar results that have been obtained but not presented, for many accident scenarios, confirm that the mathematical formulation is a satisfactory one, from the point of view of conformity with physical reality; and, that the procedure followed is reliable for gaining useful insight into industrial accidents and therefore alleviating their consequences.

Acknowledgements

The author wishes to thank Prof. D.B. Spalding and CHAM Ltd. of London, for permitting the use of the software PHOENICS with which the reported calculations were performed.

References

[1] U. Beck, The Risk Society, Sage, London, United Kingdom, 1992.
[2] L. Chang, C.C. Lin, A study of storage tanks accidents, J. Loss Prev. Process Ind. 19 (2006) 51–59.
[3] A.F. Ghoniem, X. Zhang, O. Knio, H.R. Baum, R.G. Rehm, Dispersion and deposition of smoke plumes generated in massive fires, J. Hazard. Mater. 33 (1993) 275–293.
[4] A.F. Ghoniem, X. Zhang, A computational model for the rise and dispersion of wind-blown, buoyancy driven plumes, Part I Neutrally stratified atmosphere, Atmos. Environ. 27 (1993) 2295–2311.
[5] K.B. McGrattan, H.R. Baum, R.G. Rehm, Numerical simulation of smoke plumes from large oil fires, Atmos. Environ. 30 (1996) 4125–4136.
[6] G. Miles, M. Cox, M.N. Christolis, C.A. Christidou, A.G. Boudouvis, N.C. Markatos, Modelling the environmental consequences of fires in warehouses, in: T. Kashiwagi (Ed.), Proceedings of the Forth International Symposium on Fire Safety Science, Ottawa, Canada, 1994, pp. 1221–1232.
[7] M.N. Christolis, C.A. Christidou, A.G. Boudouvis, N.C. Markatos, Modelling pollutants dispersion around buildings on fire, in: H. Power (Ed.), Proceedings of the International Conference on Air Pollution, Porto Carras, Greece, 1995, pp. 85–92.
[8] G.M. Sideris, M.N. Christolis, N.C. Markatos, Numerical simulation of pollutants dispersion around warehouses on fire, in: D.T. Tsahalis (Ed.), Proceedings of the First International Conference, From Scientific Computing to Computational Engineering, Athens, Greece, 2004.
[9] D.A. Kefalas, M.N. Christolis, Z. Nivolianitou, N.C. Markatos, Consequence analysis of an open fire incident in a pesticide storage plant, J. Loss Prev. Process Ind. 19 (2006) 78–88.
[10] C.D. Argyropoulos, M.N. Christolis, N.C. Markatos, Z. Nivolianitou, Assessment of acute effects for fire-fighters during a fuel-tank fire, in: Proceedings of the 4th International Conference on Prevention of Occupational Accident in a Changing Work Environment, WOS 2008, 30 September–3 October 2008, Crete, Greece.
[11] N.C. Markatos, Mathematical modelling of single- and two-phase flow problems in the process industries, Oil & Gas Sci. Technol. – Rev. IFP 48 (1993) 631–662.
[12] W.K. Anderson, J. Thomas, B. Van Leer, Comparison of finite volume flux vector splittings for the Euler equations, AIAA J. 24 (1986) 1453.
[13] M.K. Patel, M. Cross, N.C. Markatos, An assessment of flow oriented schemes for reducing false diffusion, Int. J. Numer. Meth. Eng. 26 (1988) 2279.
[14] D.B. Spalding, Mathematical modelling of fluid-mechanics, heat-transfer and chemical-reaction processes, A Lecture Course, CFDU Report, HTS/80/1, Imperial College, London, 1980.
[15] N.C. Markatos, K.A. Pericleous, Laminar and turbulent natural convection in an enclosed cavity, Int. J. Heat Mass Transfer 27 (5) (1984) 755–772.
[16] V. Yakhot, S.A. Orszag, Renormalization group analysis of turbulence I. Basic theory, J. Sci. Comput. 1 (1986) 3–51.
[17] R. Siegel, J.R. Howell, Thermal radiation heat transfer, 4th ed., Hemisphere, Washington, 2002.;
E.P. Keramida, H.H. Liakos, M.A. Founti, A.G. Boudouvis, N.C. Markatos, Radiative heat transfer in natural gas-fired furnaces, Int. J. Heat Mass Transfer 43 (2000) 351–371.
[18] F.C. Lockwood, N.G. Shah, A new radiation solution method for incorporation in general combustion prediction procedures, in: Proceedings of the Eighteenth Symposium (Inter.) on Combustion, The Combustion Institute, Pittsburgh, 1981, pp. 1405–1416.
[19] H.M. Kim, V.C. Patel, Test of turbulence models for wind flow over terrain with separation and recirculation, Bound. Layer Meteorol. 94 (2000) 5–21.
[20] H. Tennekes, The logarithmic wind profile, J. Atmos. Sci. 30 (1973) 234–238.
[21] A. Huser, P.J. Nilsen, H. Sketun, Application of k ε model to the stable ABL: pollution in complex terrain, J. Wind Eng. Ind. Aerodyn. 67 and 68 (1997) 425–436.
[22] B.E. Launder, D.B. Spalding, The numerical computation of turbulent flows, Comput. Methods Appl. Mech. Eng. 3 (1974) 269–289.
[23] V. Babrauskas, Estimating large pool fire burning rates, Fire Technol. 19 (1983) 251–261.
[24] K.A. Notarianni, D.D. Evans, W.D. Walton, D. Madrzykowski, J.R. Lawson, Smoke production from large oil pool fires, Interflam '93, Fire Safety, in: C.A. Franks (Ed.), 6th Int. Fire Conference, Oxford, England; Interscience Communications Ltd., London,, 1993, pp. 111–119.
[25] H. Koseki, Y. Iwata, Y. Natsume, T. Takahashi, T. Hirano, Tomakomai large scale crude oil fire experiments, Fire technol. 36 (2000) 24–38.
[26] D.D. Evans, G.W. Mulholland, H.R. Baum, W.D. Walton, K.B. McGrattan, In situ burning of oil spills, J. Res. Natl. Inst. Stand. Technol. 106 (2001) 231–278.
[27] W.D. Walton, W.H. Twilley, A.D. Putorti, R.R. Hiltabrand, Smoke measurements using an advanced helicopter transported sampling package with radio telemetry, in: Proceedings of the 18th Arctic and Marine Oilspill Program Technical Seminar, Environment Canada, Ottawa, Ontario, 1995, pp. 1053–1074.
[28] L.E. Booher, B. Janke, Air emissions from petroleum hydrocarbon Fires during controlled burning, Am. Ind. Hyg. Assoc. J. 58 (1997) 359–365.
[29] P.M. Lemieux, C.C. Lutes, D.A. Santoianni, Emissions of organic air toxics from open burning: a comprehensive review, Progress Energy Combust. Sci. 30 (2004) 1–32.
[30] D.D. Evans, Combustion of oil spills on water (OCS Study MMS 88-0057) Environment Canada, Reston, VA, 1991, pp. 169–179.
[31] S.V. Patankar, D.B. Spalding, A calculation procedure for heat, mats and momentum transfer in three-dimensional parabolic flows, Int. J. Heat Mass Transfer 15 (1992) 1787.
[32] D.B. Spalding, A general purpose computer program for multi-dimensional one- and two-phase flow in mathematics and computers in simulation, vol. XXIII, North Holland, Amsterdam, 1981. pp. 267–276.
[33] B. Van Leer, Towards the ultimate conservative difference scheme. A second order sequel to Godunov's method, J. Comp. Phys. 32 (1979) 101.
[34] D.B. Spalding, Novel finite-difference formulation for differential expressions involving both first and second derivatives, Int. J. Numer. Methods Eng. 4 (4) (1972) 551–559.
[35] K.B. McGrattan, H.R. Baum, A. Hamins, Thermal radiation from large pool fires, NISTIR 6546, National Institute of Standards and Technology, U.S. Department of Commerce, Washington, DC, 2000.